AIAA-2002-0917

Effective Conversion of Exit Enthalpy in a MPD Thruster

Subrata Roy[*], Pavlos Mikellides[**] and D.R. Reddy[§]

[*]CPD Laboratory, Kettering University, Flint, MI

[**]Ohio Aerospace Institute, Cleveland, OH

[§]NASA Glenn Research Center, Cleveland, OH

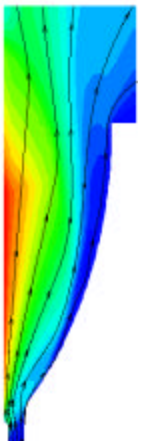

40th Aerospace Sciences Meeting and Exhibit

14-18 January 2002

Reno, Nevada

Effective Conversion of Exit Enthalpy in a MPD Thruster

Subrata Roy[*], Pavlos Mikellides[**] and Dhanireddy R. Reddy[§]

[*]*Computational Plasma Dynamics Research Laboratory*
Kettering University, Flint, MI 48504

[**]*Ohio Aerospace Institute, Cleveland, Ohio 44142*

[§]*Electric Propulsion Laboratory*
NASA Glenn Research Center, Cleveland, Ohio 44135

Acceleration of plasma by area expansion is an area of significant interest to the high power in-space propulsion research. This paper verifies the applicability of a diverging channel to designing practical self-field magnetoplasmadynamic (MPD) thruster for higher specific impulse. Theoretical development for the expanding annular geometry is documented and analyzed for a partially ionized two temperature computational model that addresses potential understanding of effect of geometric scales, and predictions of self-field magnetic effects.

INTRODUCTION:

A multiblock arbitrary coordinate hydromagnetic (MACH) family of complex geometry codes has been developed by the Center for Plasma Theory and Computation at the Air Force Research Laboratory that can study collisional plasmas. These codes are written in fortran 77, use Cray-style fortran pointers, and are designed for UNIX-type environment (see Peterkin and Frese[1]). The two and half dimensional MACH2 and the three-dimensional MACH3 are now widely being utilized to model a variety of laboratory plasma experiments such as, MARAUDER compact toroid program (Degnan et al.[2]), pulsed plasma thrusters (Turchi et al.[3]), implosion liners and MPD thrusters.

This paper focuses on the application of MACH2 code for practical magnetofluid problem by specifically documenting a design simulation of a magnetoplasmadynamic (MPD) thruster with an expansion chamber outlet. MPD thrusters are of considerable interest to the NASA Earth Science, Space Science, and Human Exploration and Development of Space Strategic Enterprises for developing high-power in-space electric propulsion system. In this device, the gaseous propellant is ionized by an arc current that interacts with the self-induced magnetic field to accelerate the plasma, and produces the required thrust through an inherently unsteady process[4-6].

Computational researchers have tried to effectively capture the physics of self-field MPD thrusters[7-9] using two-dimensional time-independent model for argon propellant. While Lapointe[7] utilized finite difference methodology to solve the fully ionized MPD equations with ideal gas equation of state, Sleziona et. Al[8] implemented the finite volume methodology for solving

[*] Assistant Professor, Department of Mechanical Engineering, E-mail: sroy@kettering.edu, Associate Fellow, AIAA
[**] Senior Research Associate, E-mail: pavlos.mikellides@oai.org, Member, AIAA
[§] Chief, On-Board Propulsion, E-mail: dreddy@grc.nasa.gov, Associate Fellow, AIAA

the velocity, pressure, electron-ion temperature and current field equations. Results in both these papers were reasonably compared with experimental thrust data.

Berry and Roy[9] developed a two-dimensional steady state algorithm utilizing a combination of the Galerkin weak statement and least squares finite element (GLS) methods for MPD applications. The Galerkin method is used to analyze the single fluid Navier-Stokes regime subjected to electromagnetic forces, while the least squares solve the electromagnetic Maxwell's equations. This *loosely-coupled* GLS algorithm allows for a very robust and mathematically complete approach. The GLS algorithm has been applied for quantitative documentation of achievable practical MPD thruster solutions.

Kawaguchi et. al[10] reported numerical solutions that included the temporal contributions via a special consideration to the difference between characteristic time scale of fluid-thermal (msec) and electromagnetic ($m$sec) effects. A detail comparison of thrust versus current curves for various mass flow rates is presented by Auweter-Kurtz et. al[11]. These results show a wide variation of numerical solution accuracy for DT series and hot anode thrusters (HAT).

Tanaka and Kimura[12] used two-dimensional electromagnetic equations with quasi-one-dimensional fluid equations to examine applied-field acceleration mechanism. The analysis showed that substantial Hall currents and plasma rotation were produced from interaction of the applied field with discharge current. For a thruster modeled with argon propellant at 0.1g/s, discharge current of 1000-2000 Amp and applied field strength of 0.1-0.2 Tesla at the cathode tip, the generated plasma rotation was converted to axial momentum via expansion through a magnetic channel.

Applications of MACH2 finite volume code in general two-dimensional unsteady plasma dynamics have been reported by Peterkin, et. al[13]. The methodology involves solutions of mass, momentum, electron and ion energy, radiation energy density, magnetic induction and elastic stress equations in arbitrary Lagrangian/Eulerian (ALE) coordinate. Recent publication of Mikellides and Truchi[14] documents the utility of this code for applied-field MPD thrusters. MACH2 has also been advocated by Mikellides et. al[15] for designing a gigawatt-level fusion propulsion system with specific impulse exceeding ten thousand seconds. In the following section, we present the block-based MACH2 numerical simulation of an annular self-field thruster with a designed expansion chamber for improved thrust.

As the area of the thruster channel expands, the plasma accelerates gradually from subsonic to supersonic velocity. At the sonic point, the compressible acceleration due to area expansion balances the deceleration due to ion and electron neutral collisions, thus avoiding the sharp singularity[16]. Manheimer and Fernsler[16] state that for a quasi-neutral nozzle plasma can accelerate to a maximum of about three times the speed of sound without any additional power supplies or fine screens in the plasma. Traditionally, MPD thrusters are limited to a low efficiency range of 25-35%[7]. The results presented in this paper document an effective design of diverging nozzle in improving the thruster efficiency to a practical 46.5%.

NOMENCLATURE:

A	= atomic weight, amu
B,**B**	= magnetic induction, Tesla
e	= elementary charge, $1.6\text{x}10^{-19}$ C
G	= shear modulus, kg/m-s^2
g	= metric tensor
I	= current, Amp
j	= current density, Amp/m^2
K	= thermal conductivity, J/m-s-eV
M	= Mach number
m	= mass of electron, $9.1\text{x}10^{-31}$ kg
n	= number density, /m^3
P	= pressure, J/m^3
Q	= numerical viscosity, J/m^3
q	= heat flux, W/m^2
T	= temperature, eV
t	= time, s
u,**u**	= flow velocity, m/s
V	= plasma voltage, V
w	= azimuthal speed, m/s
d	= Kronecker delta
e	= specific internal energy, J/kg
z	= number of free electrons/ion
g	= specific heat ratio
j	= electrical resistivity/m_0, m^2/s

μ = viscosity coefficient, kg.m-s
μ_0 = permeability in free space, H/m
n_{eq} = thermal equilibration frequency
ρ = mass density, kg/m^3
σ = stress tensor, J/m^3

Subscripts
e = electron
ex = exit condition
I = ion
L = Lagrangian step
o = neutral
r,q,z = radial, azimuthal, axial components
rad = radiation effect
s = stagnation
t = throat

NUMERICAL MODEL:

The MACH2 system of equations for single fluid unsteady, compressible flows, including continuity, momentum, the electron-ion energy model, and the magnetic field transport has been given in detail by Peterkin and Frese[1].

Continuity: $$\frac{\partial \rho}{\partial t} = -\left[u^i \nabla_i \rho + \rho \nabla_i u^i\right] \quad (1)$$

Momentum:
$$\rho \frac{\mathrm{D}u^i}{\mathrm{D}t} = \nabla_j \left[(-P+Q) g^{ij} + \frac{\sigma^{ij}}{\mu_o}\left(B^j B^i - \frac{B^2 g^{ij}}{2} \right)\right] \quad (2)$$

Electron specific internal energy:
$$\rho \frac{\mathrm{D}e_e}{\mathrm{D}t} = -P_e g^{ji} \nabla_i u^j + \eta_{ij} J^2 g^{ij} + \nabla_i \left(k_e^{ij} \nabla_j T_e\right) - \dot{q}_{rad} - \rho \nu_{el} (e_e - e_I) \quad (3)$$

Ion specific internal energy:
$$\rho \frac{\mathrm{D}e_I}{\mathrm{D}t} = \left[-(P_I + Q) g^{ji} + \sigma^{ji}\right] \nabla_i u_j + \nabla_i \left(k_I^{ij} \nabla_j T_I\right) + \rho \nu_{el} (e_e - e_I) \quad (4)$$

Magnetic induction:
$$\frac{\partial \mathbf{B}}{\partial t} = \nabla \times (\mathbf{u} \times \mathbf{B}) - \nabla \times (j \nabla \times \mathbf{B}) - \nabla \times \frac{1}{e \mu_0 n_e} (\nabla \times \mathbf{B} \times \mathbf{B}) \quad (5)$$

Equations (1)-(5) constitute a system of non-linear differential equations that is closed with the addition of an equation of state (EOS) and a caloric equation of state that prescribe the species' pressure and specific internal energy as a function of species number densities and temperatures. They can be either analytical or tabular. The analytical equations include the ideal gas model and a model appropriate for solids. The tabular database, called SESAME library (Holian[17]), includes the standard thermodynamic quantities, along with the fractional ionization state based on local thermodynamic equilibrium and transport coefficients.

In this paper, we used classical plasma resistivity model based on both electron-ion and electron-neutral collisions:

$$j = 1.0328 \times 10^{-4} \frac{z \ln \Lambda}{T_e^{3/2}} + \frac{m_e^{1/2}}{e^{3/2}} \sigma_e T_e^{1/2} \frac{1-z}{z} \quad (6)$$

For classical thermal conductivity, the Spitzer-Härm model is implemented for considering electron-ion collision frequency in which thermal conductivity for species *s* scales as

$$K_e = \frac{3.103 \times 10^4 [4.1 - 15.5/(4+z)] T_s^{5/2}}{z^2 \ln \Lambda} \quad (7)$$

where, $\ln \Lambda$ is the Coulomb logarithm. The physical model described above is solved using a time-split time-marching numerical algorithm. The Lagrangian hydrodynamics, radiation and resistive diffusion models are solved by implicit time-differencing. Corresponding convective transport, radiation cooling and the Hall effect are analyzed by explicit differencing. The code also includes various models for external electric circuits, anomalous resistivity, three different models for radiation (namely Stefan-Boltzmann, equilibrium and non-equilibrium model), and an ablation model. The spatial problem is simulated using finite volume (FV) technique.

The net thrust in the axial direction is computed as

$$T = \frac{\dot{m}}{A_e} \int_{A_e} v(r) dA_e + \int_{A_e} p(r) dA_e - p_t A_e \quad (8)$$

Corresponding specific impulse is defined as: $I_{sp} = T / \dot{m} g$ and the flow efficiency is $\eta_f = T^2 / 2 \dot{m} P$, where $P = \mathrm{VJ}$ is the power deposition in plasma for a total voltage drop V and total current J, and $\dot{m}$ is the mass flow rate of the gas. The power deposited into unit volume of plasma has two components, the power

expanded in acceleration $\mathbf{j}\times\mathbf{B}\bullet\mathbf{u}$ and the Ohmic heating j^2/s, where s is the conductivity and j is the current density.

ALE AND MULTIGRID FORMULATION

For transport through the mesh in general applications, the magneto-fluid velocity $\mathbf{u}$ in (1)-(5) is replaced by the relative velocity, $\mathbf{u}_{rel} = \mathbf{u}_g - \mathbf{u}$, where $\mathbf{u}_g$ is the grid velocity at which the boundary of the primitive cell moves. In pure Lagrangian motion, relative velocity vanishes, i.e., the fluid velocity becomes identical with the grid velocity. In arbitrary Lagrangian-Eulerian (ALE) formulation of Peterkin et. Al[13], the grid with fields supported by it are advanced during each computational cycle of incremental time, Δt in two steps. First, the grid and its fields are moved such that each node of the grid is moved by a displacement $\Delta\boldsymbol{x}_L = \mathbf{u}\Delta t$. Then, the *remapping* of each node is done using the relative velocity such that, $\Delta\boldsymbol{x} = \mathbf{u}_{rel}\Delta t$.

The corresponding FV magnetic flux advance is computed following these three steps: (1) calculate three fluxes through three Lagrangian surfaces from three Lagrangian field components for each cell; (2) redistribute the three magnetic fluxes as a response to the relative velocities of the grid and fluid; and (3) compute three new magnetic field components in each remapped cell from the three new fluxes. The diffusive process of thermal conduction and magnetic diffusion are computed in MACH2 iteratively via an implicit Jacobi method that uses a multigrid algorithm to increase the rate of convergence. The code also allows solution adaptive mesh-refinement.

THRUSTER DESIGN:

Figure 1a-b describes the schematic of a typical thruster including two electrodes, an inlet and an expanding nozzle. The numerical model consists of six computational blocks. The central cathode is of 9.5mm diameter and 45mm length with a 5mm taper in the downstream end, and the annular anode is of inner diameter 50mm. At the exit plane of these electrodes, an expanding nozzle is introduced to convert static enthalpy to axial kinetic energy for greater thrust. The height of this outlet nozzle is 205mm and at its end the maximum diameter is 178mm. Figure 1b is showing the details of the region near the electrodes.

Proper and accurate nozzle design of a magnetized, non-isentropic plasma flow with distributed heat addition that extends into the diverging section can of course only be achieved by sophisticated numerical tools, such as the MACH2 code. However, a first-iteration approximation based on simplifying assumptions can establish general nozzle dimensions and shape. Thus, if we assume isentropic flow with the sonic point at the exit of the constant-area discharge chamber we can design a diverging section that will expand the plasma flow to a desired temperature ratio.

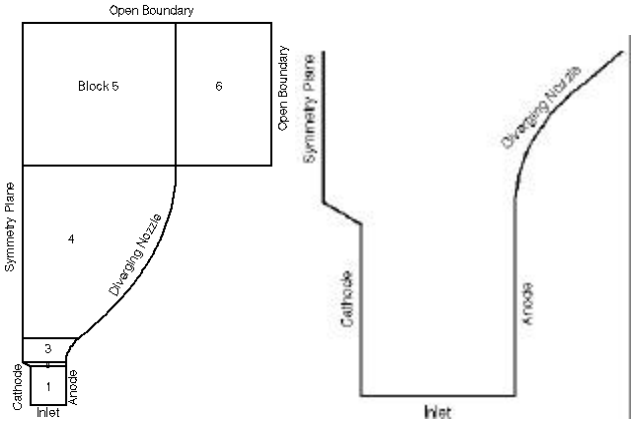

(a) Geometry (b) Zoomed near inlet

Figure 1. Schematic of the analysis domain.

Specifically, the Mach number at the exit, M_{ex} is determined by the temperature ratio, T_s/T_{ex};

$$M_{ex} = \sqrt{\frac{2}{g-1}\left(\frac{T_s}{T_{ex}} - 1\right)} \qquad (9)$$

where T_s and T_{ex} are the stagnation and exit temperatures, respectively, and γ is the ratio of specific heats. For steady-state we can approximate a magnetized plasma as a γ=2 gas, a consequence of its magnetic pressure, which in turn implies that for a temperature ratio of 30, the exit Mach number is M_{ex}=7.6. The exit Mach number defines the exit-to-throat area ratio, A_{ex}/A_t as follows (White[18]),

$$\left(\frac{A_{ex}}{A_t}\right)^2 = \frac{1}{M_{ex}^2}\left[\frac{2}{g+1}\left(1+\frac{g-1}{2}M_{ex}^2\right)\right]^{\frac{g+1}{g-1}} \qquad (10)$$

The particular nozzle simulations presented in this paper model a discharge chamber of an experimentally-tested thruster with a cathode and anode radius of 4.75 mm and 25 mm, respectively. These dimensions establish the throat area and allow calculation of the exit radius at 84 mm.

The actual contour of the diverging section is designed to assure a shock-free flow. It is generally divided into two sections; the expansion section during which the contour angle increases and a smooth "straightening" section that assures cancellation of all the expansion waves generated upstream. Traditionally, the expansion section is a circular arc of a radius larger than the throat radius with its length defined by the maximum expansion angle desired. For a minimum-length nozzle, a feature that is desirable for rocket nozzles due to weight considerations, the maximum expansion angle is half the Prandtl-Meyer function,

$$\nu(M) = \sqrt{\frac{\gamma+1}{\gamma-1}}\tan^{-1}\sqrt{\frac{\gamma-1}{\gamma+1}\left(M^2-1\right)} - \tan^{-1}\sqrt{M^2-1} \quad (11)$$

based on the design exit Mach number, $M=M_{ex}$. In this first iteration the maximum angle is 25.5º that establishes the length of the expansion section at 45mm after the radius has been chosen at twice that of the anode radius.

The remaining section's contour design is based on shock-free flow and it generally requires accurate and tedious method of characteristics. However, in this particular plasma flow we expect heat addition downstream of the chamber exhaust that will tend to diffuse shocks. Further, employing the elaborate method of characteristics for such an approximation is a redundant process, so the straightening section also employs a circular arc that is defined by the maximum expansion angle and assures a purely axial exhaust flow. Further, finer adjustments have also been made to the final shape of the diverging section in order to assure smooth grid transition.

BOUNDARY CONDITIONS:

The plasma is modeled as a real, two-temperature, viscous fluid. The real equation of state that provides the thermodynamic properties including average degree of ionization, is obtained by the semi-empirical tabular SESAME tables (Holian[17]). Radiation and the Hall effect are excluded. The following boundary conditions are applied by the ghost-cell technique. The wall boundary conditions are imposed as no-slip for the hydrodynamics and constant temperature for thermal conduction. The latter utilizes a uniform wall temperature of 1000 K for the anode and 2000K for the cathode that are typical for these power levels based on experimental measurements (Sakiyama, et. Al[19]). The inlet boundary condition prescribes uniform flow at sonic speed for a 300K Hydrogen gas at a mass flow rate of 1.37 g/s. The downstream outlet boundary conditions impose zero gradient on the pressure, internal energy, magnetic field and density. The discharge current is 10kA. The electrodes are conductors and the backplate (inlet) is an insulator. Finally, symmetry boundary condition is used at the centerline of the annular thruster geometry.

Steady-state was declared after integrated quantities such as thrust and voltage only varied within 0.1% along with qualitative interrogation of the two-dimensional distributions of the main variables. Typically, such simulations converged to state-state within 500 microsec which implies cycling through the full set of the magnetohydrodynamic equations in the excess of 100,000 times at an average timestep of less than 5 nsec.

RESULTS AND DISCUSSION:

The MACH2 code was utilized to simulate steady state, Mega-watt class MPD thruster operation. A computational mesh of 2368 finite volumes was created using MACH2 block mesh generator. MACH2 allows both Eulerian (fixed) mesh and Lagrangian (moving) mesh capability. Figure 2a shows Eulerian mesh description inside the thruster for the present problem and Figure 2b is the zoomed view of the mesh near the inlet.

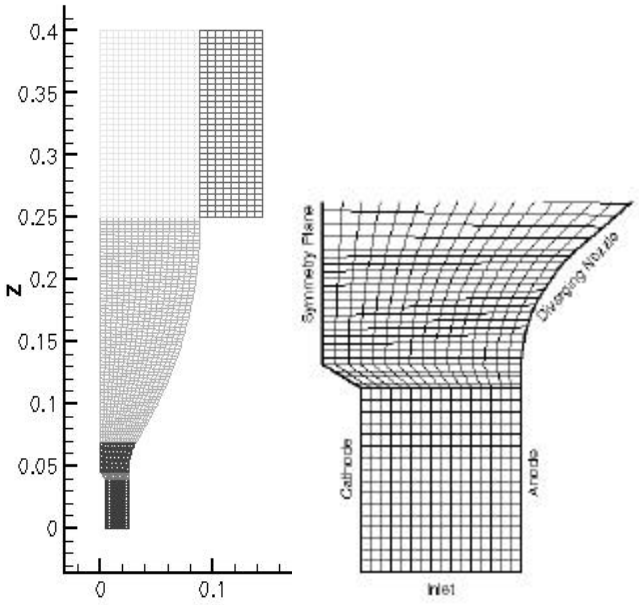

(a) (b)

Figure 2. (a) Thruster mesh; (b) Mesh near the electrodes.

Examination of the two-dimensional state variable distributions in Figures 3-7 establishes the emergence of certain physical processes that are not expected from an electromagnetic accelerator. Specifically, Figure 3a displays severe current distention downstream of the discharge chamber with values in the excess of 1000 Amps extending well into the plume region. This implies a low magnetic Reynolds number flow with a diffuse arc and thus a significant electrothermal contribution. Indeed, a comparison between the electromagnetic and electrothermal contribution to the axial kinetic power confirms an approximately 50/50 operation. This is a consequence of the electron-atom contribution to the electrical diffusivity of the plasma that in effect decreases the effective magnetic Reynolds number by two orders of magnitude. (Typically, classical diffusivity for such plasmas is of the order of 1000 m^2/s. In this particular simulation the maximum diffusivity is in the excess of 10^5 m^2/s). In turn, such operation has significant implications regarding the plasma voltage and consequently power deposition and thrust efficiency.

In addition, such distention implies continuous heat deposition into the nozzle section that impedes conversion to axial kinetic energy. This is shown in Figure 3b that displays the MACH number distribution. For the particular area-ratio expansion the exit Mach numbers (M_e) were expected to be of the order of 10 while we note that the high density plasma (see Figure 4a) does not allow M_e to exceed 3. Corresponding normal induced magnetic field is shown in Figure 4b. The inadequate static enthalpy conversion is confirmed by the two-dimensional solutions of the average degree of ionization in Figure 5, and electron and ion temperature contour plots in Figure 6a-b, respectively. Both figures show that the exhaust plasma retains substantial enthalpy into thermal and ionization modes implying that the main inefficiency is due to frozen flow losses as opposed to fall-voltage and external-circuit-element losses.

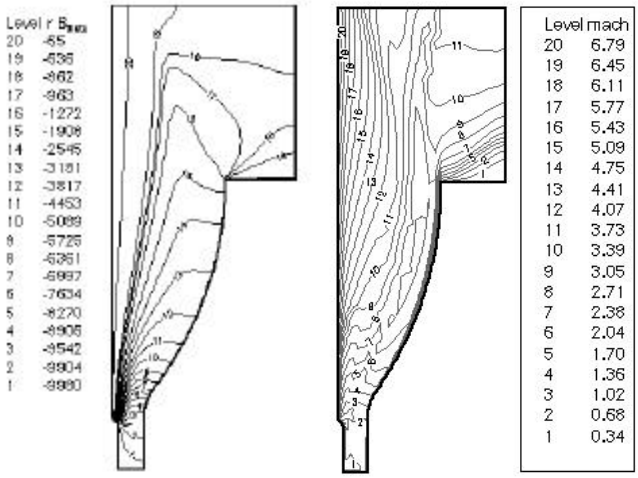

(a) Current (rB_θ) (b) Mach number

Figure 3. MACH2 solution contours.

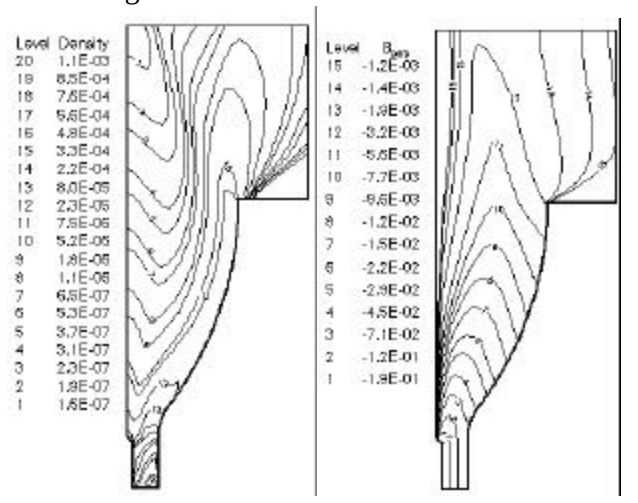

(a) Density (b) Magnetic field ($B_\perp$)

Figure 4. MACH2 solution contours.

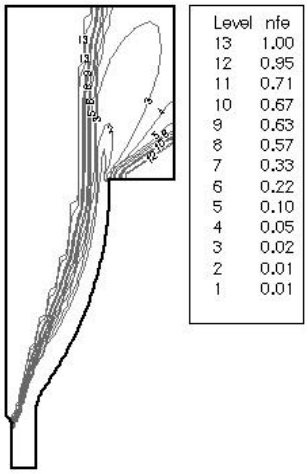

Figure 5. Average degree of ionization.

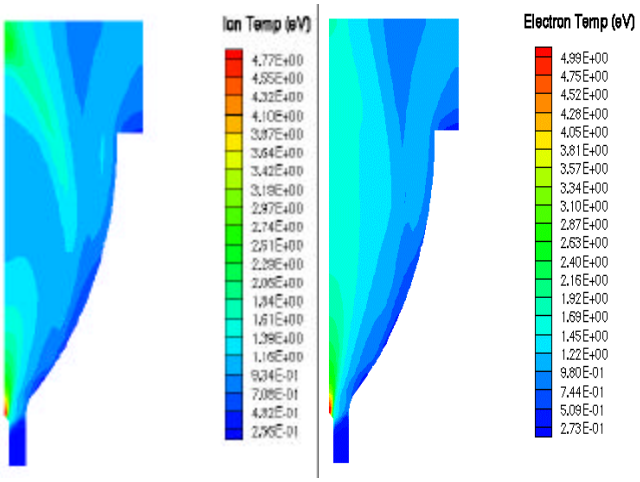

(a) Electron temperature (b) Ion Temperature

Figure 6. Temperature solution contours.

The radial (u_r) and axial (u_z) components of fluid velocity distributions are plotted in Figure 7. Five individual particle tracks are superimposed to show the dominance outward radial velocity component in the nozzle section (see Figure 7a). Noticeably Figure 7b shows the least axial velocity in the high density plasma regions of Figure 4a, documenting a pinching effect from the radial component of the electromotive force ($\vec{J} \times \vec{B}$).

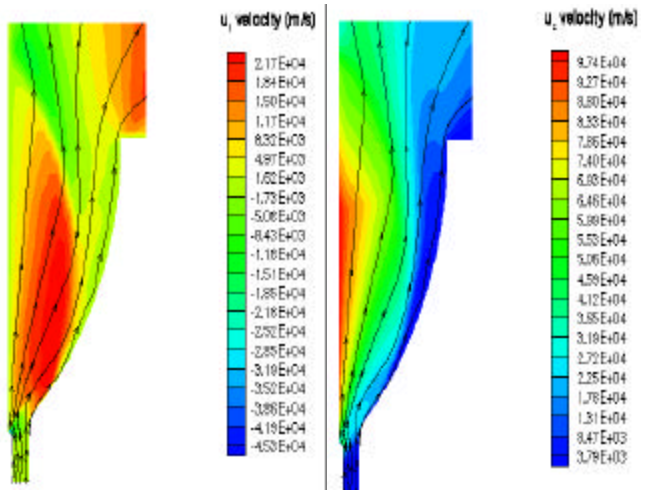

(a) u_r (b) u_z

Figure 7. Radial and axial components of fluid velocity.

The variation of ion (t_{ion}) and electron temperature (t_e), density and magnetic field (B_θ) along the axial direction of the thruster are plotted on three different radial locations r = 0.01, 0.014 and 0.018 in Figure 8. Both ion and electron temperature increases drastically in the near-region of the expansion chamber, i.e., block 3 and inlet section of block 4 (see Figure 1a). The rest of domain essentially remain invariant for these three radial locations. An efficient conversion of this high exit enthalpy to acceleration will result in higher thruster efficiency. The azimuthal magnetic field and plasma density show variation in the field in the main thruster channel, i.e., block 1 and 2 in Fig. 1.

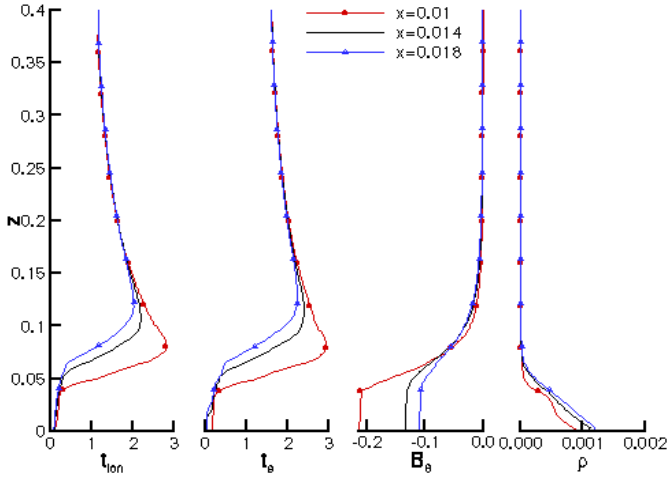

Figure 8. Thruster simulation detail at three radial locations.

Finally, the MPD thruster performance is summarized in Figure 9. The radial $(J \times B)_r$ and axial $(J \times B)_z$

components of the electromotive force, and the thrust components (T_r and T_z) converge to steady state after about 350 micro seconds. For 1.37 g/s atomic hydrogen and an applied current of 10kA, the integrated axial thrust via (8) is 50.5N and the calculated specific impulse is 3757.5s. Corresponding flow efficiency is calculated as 46.5%. Corresponding discharge voltage at steady state is 200V.

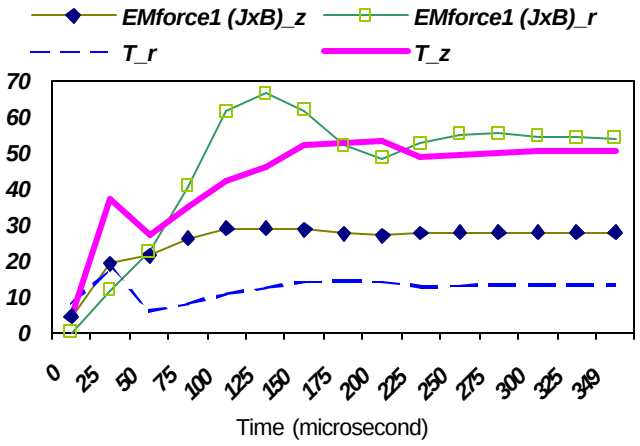

Figure 9. Thruster performance summary for 1.37g/s H.

CONCLUSIONS:

This paper verifies the applicability of the MACH2 finite volume research code to designing practical self-field MPD thruster. Theoretical development for a diverging annular geometry is documented and analyzed for a partially ionized two temperature computational model that addresses potential understanding of effect of geometric scales, and predictions of self-field magnetic effects. Presented results document the thrust advantage of plasma acceleration due to area expansion.

ACKNOWLEDGEMENTS:

This work started during the first author's tenure at Glenn Research Center as a NASA/OAI Collaborative Research Fellow during the summer of 2000 and was later partially supported by the NASA research grant no. NAG3-2638. The authors gratefully acknowledge many thoughtful discussions with Dr. Michael Lapointe.

REFERENCES:

[1]Peterkin, R.E., Jr. and Frese, M.H., MACH: A Reference Manual – First Edition, Air Force Research Laboratory, Kirtland AFB, New Mexico, September 14, 1998.

[2]Degnan, J.H., Peterkin, R.E., Jr., Baca, G.P., Beason, J.D., Bell, D.E., Dearborn, M.E., Dietz, D., Douglas, M.R., Englert, S.E., Englert, T.J., Hackett, K.E., Holmes, J.H., Hussey, T.W., Kiuttu, G.F., Lehr, F.M., Marklin, G.J., Mullins, B.W., Price, D.W., Roderick, N.F., Ruden, E.L., Sovinec, C.R., Turchi, P.J., Bird, G., Coffey, S.K., Seiler, S.W., Gale, D., Graham, J.D., Scott, M., and Sommars, W., Physics of Fluids B, Vol. 5, 1993, pp. 2938.

[3]Turchi, P.J., Mikellides, I.G., Mikellides, P.G. and Kamhawi, H., "Pulsed Plasma Thrusters for Microsatellite Propulsion: Techniques for Optimization," Micropropulsion for Small Spacecraft, Progress in Astronautics and Aeronautics, Hardcover ISBN: 1563474484 , 2000.

[4]Chen, F.F., Plasma Physics and Controlled Fusion, Plenum Press, 1984.

[5]Hastings, D.E. and Niewood, E.H., "Theory of the modified two-stream instability in a magnetoplasma-dynamic thruster," Journal of Propulsion and Power, Vol. 7, No. 2, pp. 258-268, 1991.

[6]Choueiri, E.Y., *Electron-ion Streaming Instabilities of an Electromagnetically Accelerated Plasma*, PhD dissertation, Princeton University, 1991.

[7]Lapointe, M., "Numerical simulation of self-field MPD thrusters," AIAA Paper No. 91-2341, 1991.

[8]Sleziona, P.C., Auweter-Kurtz, M., and Schrade, H.O., "Computation of MPD flows and comparison with experimental results," Int. Journal for Numerical Methods in Engineering, Vol. 34, pp. 759—771, 1992.

[9]Kawaguchi, H., Sasaki, K., Itoh, H., and Honma, T., "Numerical study of the thrust mechanism in a two-dimensional MPD thruster," Int. Journal of Applied Electromagnetics and Mechanics, Vol. 6, pp. 351--365, 1995.

[10]Auweter-Kurtz, M., Boie, C., Kaeppeler, H.J., Kurtz, H.L., Schrade, H.O., Sleziona, P.C., Wagner, H.P., and Wegmann, T, "Magnetoplasmadynamic thrusters: design criteria and numerical simulation," Int. J. of Applied Electromagnetics in Materials, Vol. 4, pp. 383-401, 1994.

[11]Berry, K.J., and Roy, S., Least Square FE Based MPD Algorithm for Practical Magnetoplasma

Applications, AIAA 39th Aerospace Sciences Meeting, AIAA-2001-0200, Jan. 2001.
[12]Tanaka, M., and Kimura, I., "Current distribution and plasma acceleration in MPD arcjets with applied magnetic fields," Journal of Propulsion and Power, Vol. 4, No. 5, pp. 428-436, 1988.
[13]Peterkin, R.E., Jr., Frese, M.H., and Sovinec, C.R., "Transport of magnetic flux in an arbitrary coordinate ALE code," Journal of Computational Physics, Vol. 140, pp. 148-171, 1998.
[14]Mikellides, P.G., and Turchi, P.J., "Applied-field magnetoplasmadynamic thrusters, Part 1: Numerical simulations using the MACH2 code," Journal of Propulsion and Power, Vol. 16, No. 5, pp. 887-893, 2000.
[15]Mikellides, P.G., Turchi, P.J., and Mikellides, I.J., "Design of a fusion propulsion system, Part 1: Gigawatt-level magnetoplasmadynamic source," Journal of Propulsion and Power, (in review).
[16]Manheimer, W.M. and Fernsler, R.F., "Plasma acceleration by area expansion," IEEE Transactions on Plasma Science, Vol. 29, no. 1, 2001, pp. 75-84.
[17]Holian, K.S. (Ed.), T-4 Handbook of Material Properties Database, Vol. Ic:EOS, LA-10160-MS, Los Alamos National Laboratory, Los Alamos, NM, Nov. 1984.
[18]White, F.M., *Viscous Fluid Flow*, McGraw Hill, 1974.
[19]Sakiyama, T., Iwai, A., Yoshiwa, M., Yoshida, R., Kagaya, Y., Wasa, T., Tahara, H. and Yoshikawa, T., "Continuous operation test of quasi-steady MPD thruster," AIAA 87-1045, 1987.